RESEARCH ARTICLE

# Optimization of corn screening device based on high-precision aerodynamic model

Lijuan Cheng[1,*], Qianglong He[2], Jiangru Pan[1], Jianmin Liu[3]

[1]School of Control Engineering, Xinjiang Institute of Engineering, Urumqi, Xinjiang, China. [2]Department of Mechanical and Electrical Engineering, Xinjiang Industrial Vocational and Technical College, Urumqi, Xinjiang, China. [3]Jiuquan OK Seed Machinery Co., Ltd, Jiuquan, Gansu, China.

**Received:** December 11, 2023; **accepted:** February 7, 2024.

**Mechanized agriculture is the foundation of large-scale agriculture. However, in current mechanized corn cultivation, the cleaning efficiency during the cleaning phase is poor due to design defects, which in turn reduces its yield. Therefore, this study proposed an optimization of the corn screening device based on high-precision aerodynamic models. 3D modeling was used to explore the parameter optimization of the corn cleaning devices from an aerodynamic point of view, and certain improvements were made to the fish scale sieve structure. The results indicated that the cleaning efficiency was related to airflow velocity, vibration frequency, and the opening of the fish scale sieve. The optimal wind speed was 16 m/s, and the separation efficiency currently was 94.27%. The optimal vibration frequency was 8 Hz, and the separation efficiency currently was 97.24%. The optimal opening of the fish scale sieve was 26 mm, at which point the screening efficiency reached 100%. The optimized fish scale sieve reduced blockage by 63.7% compared to the traditional fish scale sieve, and ultimately achieved an impurity content of 1.4% with an improvement of 81.3%. In summary, the optimization plan proposed by this research can effectively improve the cleaning efficiency of corn and promote agricultural production and efficiency.**

**Keywords:** corn harvest; cleaning; vibration frequency; air flow velocity; sieving.

[*]**Corresponding author:** Lijuan Cheng, School of Control Engineering, Xinjiang Institute of Engineering, Urumqi 830000, Xinjiang, China. Email: chenglj2023@163.com.

## Introduction

Agriculture, as a pillar industry of China, plays an important role in ensuring people's livelihoods and national stability [1]. Corn, as a widely cultivated food crop, is of crucial importance for the food security of the country [2]. As the quality of life improves, people's demand for corn continues to increase, which also promotes the expansion of the planting scale of corn [3]. To meet the growing demand, the planting and harvesting methods of corn also require the support of high-tech mechanization [4]. The entire mechanization of corn planting can significantly improve production efficiency, reduce labor costs, and improve the production environment for farmers [5]. During harvesting, high-tech mechanization mainly refers to the use of corn harvesters. The mechanized equipment can automatically complete tasks such as corn cutting, threshing, and cleaning, greatly improving harvesting efficiency and reducing losses [6]. For traditional corn mechanized cleaning operations, the high loss rate and low screening rate have become significant challenges.

Mechanized agriculture is a mode of agricultural production that utilizes mechanical equipment and technology to replace human labor. It plays an important role in the agricultural sector and is important for the efficiency, quality, and sustainable development of agricultural production. It can improve agricultural production efficiency, the working conditions of farmers, and enhance product quality and market competitiveness. Rakhra *et al*. analyzed the use of machinery in modern mechanized agriculture and proposed the three basic energy sources of agricultural mechanization including mechanical power, animal power, and manpower. They proposed suggestions for the reform of agricultural mechanization by analyzing the advantages and disadvantages of the three major energy sources in mechanized agriculture, which provided a theoretical basis for the further development and improvement of agriculture [7]. Adhikari *et al*. conducted a study on the spatial variability of soil in modern corn cultivation. The years of yield monitoring data and geological statistical techniques were used to investigate the spatiotemporal stability and variability of corn. The study identified areas in each farmland that were not suitable for planting, and the stable yield areas and non-profit areas were designated. This study had a positive impact on improving the economic benefits of farmers and could provide data and theoretical support for the economic benefits of environmental protection [8]. Yao *et al*. proposed an automatic detection system for rice light induced pests targeting agricultural diseases and pests. An automatic processing of pests and diseases in farmland had been achieved by combining machine learning methods. These experiments confirmed the effectiveness of the method for pests and diseases [9]. Shubha et al. proposed a controlled transport agriculture method to optimize mechanized farming of crops by reducing the area in response to the soil compaction in mechanized farming. The results demonstrated the effectiveness of this method, resulting in a significant increase in crop yield [10]. Nassani *et al*. explored clean energy in mechanized agriculture and examined the carbon emission pollution data. The study emphasized the importance of sustainable mechanized agriculture and provided theoretical support for achieving sustainable environmental development [11].

Cleaning refers to the process of screening, sorting, and removing impurities from agricultural products. The purpose of cleaning is to improve the quality of produce and reduce the amount of impurities. Advanced cleaning is an evaluation indicator for agricultural and industrial modernization. Cleaning is crucial for the quality control of agricultural products. It not only provides consumers with a better product experience, but also has a positive impact on farmers' income and market competitiveness. Owen *et al*. addressed the problem of weeds in crop seeds starting from the pre-planting stage and adopted a cleaning method to determine the contamination of crop seeds by weeds. The results demonstrated the effectiveness of crop seed cleaning in improving yield [12]. Frischie *et al*. conducted an in-depth study of the specific methods and effects of crop seed cleaning, exploring the impact of cleaning on the lifespan and quality of seeds. Suggestions were proposed for seed-cleaning, emphasizing the necessity of conducting seed cleaning work before planting operations, which provided reference values for the selection of crop seeds and could effectively promote the improvement of crop yield [13]. Aradwad *et al*. proposed a solar powered multi-crop screen cleaner to improve crop cleaning efficiency. The results confirmed the effectiveness of this method for soybeans, lentils, and chickpeas, which could effectively achieve the cleaning of legume crops and had high separation efficiency and extremely low impurity content. This method had a positive effect on the clean energy utilization of mechanized agriculture [14]. Esteso *et al*. proposed a crop planning approach that considered crop cleaning steps to address the supply chain inequality in traditional agriculture. These experiments confirmed the effective help of this method in promoting supply chain fairness, providing theoretical support for promoting agriculture

[15]. Suardi *et al*. designed a combined grain cleaning system with a harvester to address the recovering husks from cereal crops. The recovery of husks was achieved by combining a turbine to collect husks discharged from the cleaning system. This device could effectively recover and package the husks. The results confirmed that this method had a positive promoting effect on improving the utilization rate of agricultural by-products and increasing agricultural income [16]. The cleaning of corn is the final step before it can enter the grain depots, and the cleaning operation is also an important link in the mechanized corn harvesting process that incurs losses. The efficiency of the cleaning operations has an extremely important impact on the overall efficiency of harvesting. The screening mechanism of corn mainly receives mixed corn materials after threshing [17]. Mixed materials often exhibit significant mass unevenness, and different mass distributions can affect the cleaning efficiency in different regions of the cleaning screen, thereby affecting the efficiency of the entire cleaning process. Conventional corn cleaning mechanisms typically rely mainly on airflow, which separates the mixed corn materials and to some extent drives some of the materials to migrate backwards, in conjunction with equipment to achieve corn cleaning operations.

Traditional cleaning operations in current mechanized agriculture still suffer from serious efficiency issues. There is significant optimization space for the impurity content and loss rate of the cleaning. Therefore, this study proposed to optimize the corn screening device based on high-precision aerodynamic models. By studying the cleaning mechanism using aerodynamics, the specific mechanism of cleaning and the reasons for blockage were explored, and targeted improvements were made to overcome the high impurity and loss rates in cleaning corn. By improving the device, the cleaning efficiency of corn could be effectively improved, ensuring its high yield and efficiency. This research could directly improve the efficiency of corn harvesting and the quality of cleaning, which was crucial to ensuring the country's food security. Further, it could reduce resource waste and improve the sustainability of overall food production by reducing the loss rate of corn cleaning selection.

## Materials and Methods

### Modeling and analysis of corn screening device

Based on corn cleaning system, high-precision aerodynamic modeling was conducted to analyze the cleaning mechanism of contents and the factors that affected its efficiency, which could be effectively improved. By the force of airflow, corn grains could be separated from impurities. As an important component factor in the cleaning process, exploring the cleaning mechanism of airflow was of great significance [18]. The SolidWorks software (Dassault Systèmes, Vélizy-Villacoublay, France) was first used to model the corn cleaning device to establish the three-dimensional model of the corn cleaning mechanism (Figure 1). The model was then imported into Workbench ICEM for grid partitioning to achieve higher accuracy, and important cleaning components such as the fish scale sieve and tail sieve that were locally grid dense. The air inlet was set as the pressure inlet of the model, and the outlet of the tail screen was set as the pressure outlet. The airflow model specifically adopted the standard $k-\varepsilon$ turbulence model [19]. When the airflow passed through the mixed material, the resistance coefficient was as follows.

$$C_m = \frac{(\rho_m - \rho_a)(1-\varepsilon_m)T_m g}{2\rho_a v^2} \quad (1)$$

where $\rho_m$ was the density of corn particles. $\rho_a$ was the air density. $\varepsilon_m$ was the stacking porosity of the mixture layer. $T_m$ was the stacking thickness of the material layer. $g$ was the acceleration of gravity. $v$ was the airflow velocity in the fan. Under the action of airflow, material particles would undergo jumping motion relative to the surface of the fish scale

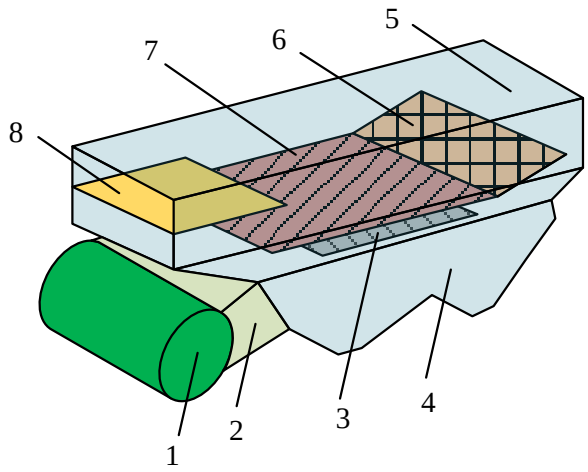


1. Air inlet
2. Air distributor
3. Lower fish scale sieve
4. Clean the exterior shell
5. Tail sieve
6. Air outlet
7. Top fish scale sieve
8. Vibrating board

**Figure 1.** Three-dimensional model of corn cleaning mechanism.

sieve. The direction parallel to the fish scale sieve was set as $x$ axis, and the direction perpendicular to the fish scale sieve was set as $y$ axis to analyze the jumping motion state of material particles more intuitively. A two-dimensional coordinate system was established to analyze its motion state. When the material particles underwent jumping motion, their relative acceleration along $x$ and $y$ axes could be determined as follows.

$$\begin{cases} a_{mx} = k\rho Sv^2\cos(\alpha-\delta)+mA\omega^2\sin(\omega t)\cos(\theta-\delta)-g\sin\delta \\ a_{my} = k\rho Sv^2\sin(\alpha-\delta)+mA\omega^2\sin(\omega t)\cos(\theta-\delta)-g\cos\delta \end{cases} \quad (2)$$

where $\alpha$ was the angle between the airflow of the fan and the horizontal direction. $\delta$ was the inclination angle of the teeth of the fish scale sieve. $\theta$ was the direction angle of inertia force during vibration. If the initial phase of the crank rotation during the first jump of the material particle was $\varphi_0$, the initial phase could be represented as the starting angle of the material particle's jump motion, which could be calculated by formula (3).

$$\varphi_0 = \arcsin\left(\frac{\frac{\cos\delta}{\sin(\alpha-\delta)}-k\rho Sv^2\frac{\sin(\theta-\delta)}{\sin(\alpha-\delta)}}{\frac{A\omega^2}{g}}\right) \quad (3)$$

If the crank rotation stop phase of the material particles at the end of the first jumping motion was $\varphi_1$, the jumping time of the particles could be calculated by formula (4).

$$\Delta t = \frac{\varphi_1-\varphi_0}{\omega} = \frac{\omega t-\varphi_0}{\omega} \quad (4)$$

The relative motion displacement of the material particles in both directions after the jump could be obtained by integrating the jump time with relative acceleration. Formula (5) represented the relative motion displacement in the horizontal direction.

$$S_x = -\frac{1}{2}g\left(\sin\delta-k\rho Sv^2\cos(\alpha-\delta)\right)\left(\frac{\varphi_1-\varphi_0}{\omega}\right)^2 - A\cos(\theta-\delta)\left[\sin\varphi-\sin\varphi_0-\cos\varphi_0(\varphi_1-\varphi_0)\right] \quad (5)$$

Meanwhile, the relative motion displacement in the vertical direction was determined by formula (6).

$$S_y = -\frac{1}{2}g\left(\cos\delta-k\rho Sv^2\cos(\alpha-\delta)\right)\left(\frac{\varphi_1-\varphi_0}{\omega}\right)^2 - A\sin(\theta-\delta)\left[\sin\varphi-\sin\varphi_0-\cos\varphi_0(\varphi_1-\varphi_0)\right] \quad (6)$$

After a jump of the material particles from the fish scale sieve surface, the horizontal displacement from the beginning to the end was

determined by formula (7), while the vertical displacement was determined by formula (8).

$$S_H = S_x \cdot \cos\delta \quad (7)$$

$$S_V = S_y \cdot \sin\delta \quad (8)$$

When the material particles completed the jumping motion and fell onto the fish scale sieve surface, the horizontal motion speed relative to the sieve surface and the relative velocity of vertical motion could be expressed as formulas (9) and (10), respectively.

$$v_x^{'} = -g\left(\sin\delta - k\rho S v^2\cos(\alpha-\delta)\right)\left(\frac{\varphi_1-\varphi_0}{\omega}\right) - A\cos(\theta-\delta)(\cos\varphi_1-\cos\varphi_0) \quad (9)$$

$$v_y^{'} = -g\left(\cos\delta - k\rho S v^2\cos(\alpha-\delta)\right)\left(\frac{\varphi_1-\varphi_0}{\omega}\right) + A\sin(\theta-\delta)(\cos\varphi_1-\cos\varphi_0) \quad (10)$$

When the material particles jumped from the fish scale sieve surface under external forces, their overall trajectory mainly presented a parabola through the analysis of formulas (2) - (10). The horizontal and vertical displacements were mainly related to the vibration frequency, vibration amplitude, wind force, and the inclination angle of the sieve teeth. Therefore, during the cleaning operation, the vibrational frequency, wind force magnitude, and vibrational amplitude could be adjusted to interfere with the jumping motion of particles and optimize the cleaning efficiency.

**Optimization of corn screening mechanism**

In practical cleaning operations, the most ideal condition is that all the corn particles pass through the screen, while all other impurities are eliminated. However, the blockage of the core shaft of corn is very serious in reality, which reduces the effective area of the sieve surface and the efficiency of screening, causing some grains to be unable to be screened normally. On the other hand, the blockage hinders the transmission of airflow and reduces the flow and uniformity of airflow in the sieve surface, thus affecting the screening and leading to a decrease in screening efficiency and an increase in impurity content. After the core shaft falls into the sieve hole, it is continuously compressed and deformed due to compression. Finally, the core shaft slides downwards along the direction of the fish scale sieve, ultimately blocking the sieve hole. The upper and lower screens in the fish scale sieve generated squeezing forces $F_k$ and $F_{k'}$ on them, respectively. After being squeezed, the core shaft underwent deformation, and ultimately its radius was less than $r$. At this point, the friction force of the core shaft could be expressed by formula (11).

$$\mu F_k = \mu F_{k'} = \mu E \cdot \frac{L}{A} \cdot \Delta L = \mu E \cdot \frac{L}{A}(L-r) \quad (11)$$

where $L$ was the mesh size of the fish scale sieve. $E$ was the surface elastic modulus of the core shaft. $r$ was the size of the core shaft. $\mu$ was the coefficient of friction. $r^{'}$ was the size of the core shaft after extrusion. Formula (12) was the equilibrium equation of the core shaft along the direction of the fish scale sieve teeth, while formula (13) was the balance equation in the vertical direction.

$$F_x = mg\cos\delta + mA\omega^2\sin(\omega t)\sin\beta - k\rho S v^2\sin\delta \quad (12)$$

$$F_y = mg\sin\delta - mA\omega^2\sin(\omega t)\cos\beta - 2\mu E\cdot\frac{L}{A}\cdot(L-r) - k\rho S v^2\cos\delta \quad (13)$$

where $m$ was the mass of the core spindle. $\beta$ was the vibration angle of the screen surface. $\delta$ was the inclination angle of the sieve teeth of the fish scale. $g$ was the acceleration of gravity. $A$ was the amplitude of the sieve surface. $k$ was the floating coefficient of the material. $S$ was the windward force area. $\rho$ was the air density. $v$ was the airflow velocity. Under the action of gravity, the core shaft continuously moved downwards at the sieve opening, and the squeezing force that it received continuously

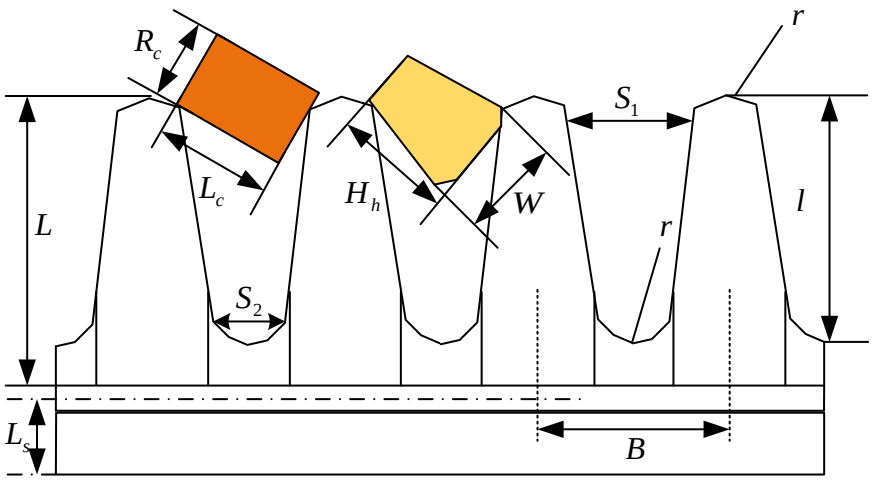


**Figure 2.** Schematic diagram of the actual situation of fish scale sieve. ***L:*** the length of the sieve teeth of the fish scale sieve. ***Ls:*** the length of the bottom base of the fish scale sieve. ***l:*** the length of the curved mesh of the fish scale sieve. ***B:*** the spacing of sieve holes between adjacent fish scales. ***r***: the minimum radius of the sieve opening. $S_1$: the uppermost distance of the curved sieve opening. $S_2$: the lowest distance of the curved sieve opening.

increased. When the pressure reached a certain threshold, the core shaft was no longer able to be eliminated by vibration and fan airflow, resulting in complete blockage at the fish-scale sieve hole. To address this issue, the structural parameters of the fish-scale sieve were re-optimized. When redesigning the fish scale sieve, it was necessary to reconfirm the distance $S_1$ from the upper end of its sieve hole, which should be greater than the maximum size of the grain (Figure 2). The required screening distance was maximized when the corn seed particles were tilted into the upper part of the sieve. At this point, the minimum distance of $S_1$ must be greater than the diagonal length of the corn seed particle as formula (14).

$$S_1 > \sqrt{W_2^2 + H_h^2 + T^2} \quad (14)$$

where $W$ was the maximum top and bottom width of the corn seed particle. $H_h$ was the maximum height of the corn seed particle. $T$ was the maximum thickness of the corn seed particle. Based on the maximum size data of the corn seed particle obtained through statistics, the minimum $S_1$ could be obtained by substituting it. When determining the minimum distance to the bottom, it was necessary to ensure that the core shaft did not penetrate the sieve at the bottom of the sieve hole, so $S_2$ should meet the minimum size larger than the core shaft. When the core shaft passed through the sieve hole along the shortest radius direction, its distance was the shortest and was represented by formula (15).

$$S_2 > \min(R_C, L_C) \quad (15)$$

where $R_C$ was the radius of the mandrel. $L_C$ was the length of the spindle. By calculating the size of the mandrel and substituting it into the formula, the optimal $S_2$ design size could be obtained. The structure of the fish scale sieve was optimized to further improve the cleaning efficiency. A schematic diagram of the shape of the teeth of the traditional fish scale sieve and the optimized fish scale sieve was demonstrated in Figure 3. In traditional fish scale screens, the teeth on the fish scale screens form a certain bending angle with their tail substrate. As the airflow passes through the fish scale sieve at a certain angle, the curved shape in the structure will cause the airflow to form multiple vortex regions, thereby increasing the resistance to the airflow. This is a significant consumption caused

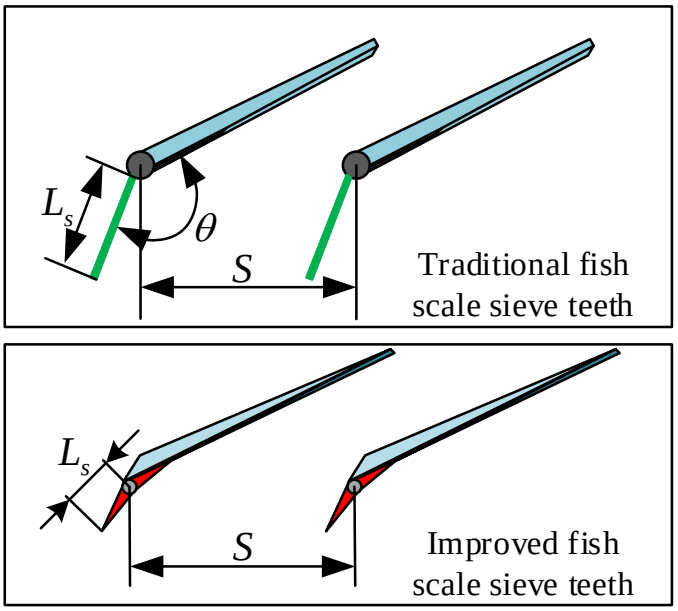


**Figure 3.** Diagram of improving the structure of fish scale screen teeth.

by the thrust of the airflow, which in turn affects the cleaning [20]. Therefore, the mesh structure of the fish scale sieve was optimized and transformed in response to this issue. The study redesigned the curved part of the tooth structure of the traditional fish scale sieve, replacing the bending structure in the traditional fish scale sieve with a smoother transition. The modified fish scale sieve teeth structure could provide good guidance for airflow below. The formation of eddy currents was effectively avoided by increasing the angle between the sieve teeth and the substrate, thereby reducing the blocking effect of the fish scale sieve on the airflow, which reduced the resistance of the airflow, improved the airflow flow rate, effectively increased the airflow utilization rate in the cleaning operation, and improved the cleaning efficiency.

To further validate the optimization scheme of the corn screening device, SolidWorks was used to model the corn screening device and further construct simulated corn seed particles, mandrels, and stem models. The input amount of corn was set to 8 kg/s, and the input amount of corn cleaning mixed materials was 5.6 kg/s. The proportion of each component in the mixed materials were determined, and the number of corn seed particles, mandrels, and stems could be simulated. For both screenings, tests were carried out throughout the harvest season in Changji, Xinjiang, China to ensure the reliability of the results. Both screens were installed on the same type of harvesters to ensure consistent test conditions. During harvesting, the sieve was regularly checked and recorded for the content of clogging substances and impurities. The difference between the two sieves was then compared.

## Results and discussion

### The effect of airflow velocity on material dispersion

The airflow velocities of 8, 10, 12, 14, and 16 m/s were selected to test the dispersion of corn grains at different cleaning times. The results showed that overall dispersion of the material appeared to be the best when the velocity of the flow was 16 m/s. As the cleaning time increased, the degree of dispersion increased first and achieved the highest degree of material dispersion as 94.27% when the cleaning time

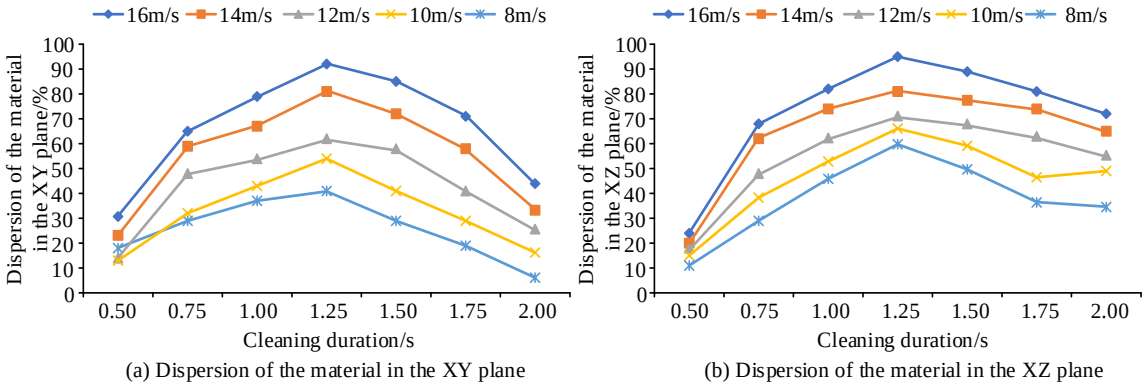


**Figure 4.** Comparison of the influence of different airflow velocity on dispersion.

reached 1.25 s, which was 11.19 - 67.38% higher than that of other velocities of the flow. However, when the cleaning time was further increased, the dispersion was decreased (Figure 4).

**The efficiency of the vibrating screen at different airflow velocities**

At an airflow speed of 16 m/s, the screening efficiency of the vibrating screen reached a maximum of 97.24% at a cleaning time of 2.50 s, which was 17.24 - 49.98% higher than the screening efficiencies under other parameter settings (Figure 5). The vibrational frequencies were then investigated at 4, 5, 6, 7, and 8 Hz. The dispersion of materials under different vibration frequencies was tested. The results demonstrated that, when the vibration frequency was 8 Hz, the overall material dispersion performance was optimal. The dispersion of the material increased with the increase of cleaning time until 1.25 s, at which the dispersion degree of the material performed the best, reaching 95.27%, which was 17.21 - 49.68% higher than that of other parameter settings (Figure 6). The effect of different vibration frequencies on the screening efficiency of the vibrating screen was investigated. The results showed that, at a screening time of 2.50 s, the screening efficiency at 4 Hz achieved the best performance at 98.27%, which was 2.24 - 4.57% higher than that of other parameters. However, at a screening time of 1.25 s, the screening efficiency at 7 Hz reached the best performance at 68.25%, which was 9.28 - 21.32% higher than that of the other parameters. Overall, the screening efficiency at 4 Hz, 2.50 s was the best option with the screening efficiency reaching 98.27% (Figure 7).

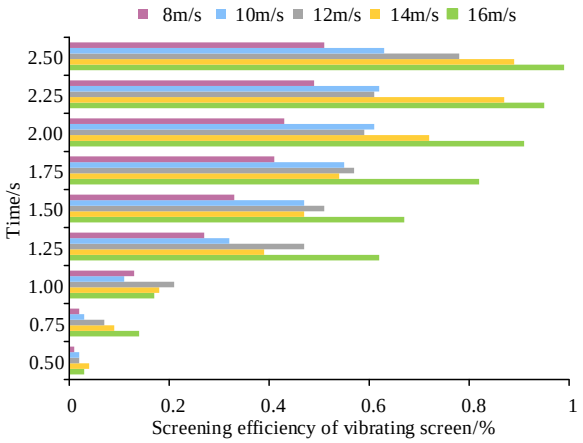


**Figure 5.** Comparison of screening efficiency of vibrating screen at different airflow speeds.

**The effect of the fish scale sieve angles on the screening efficiency**

The opening and closing angles of the fish scale sieve were set to 18, 20, 22, 24, and 26 mm. When the opening of the fish scale sieve was set at 26 mm, its overall screening efficiency reached the best result of 100%, which was 3.27 - 7.38% higher than that of the other parameters. The screening efficiency increased with the increase of screening time (Figure 8).

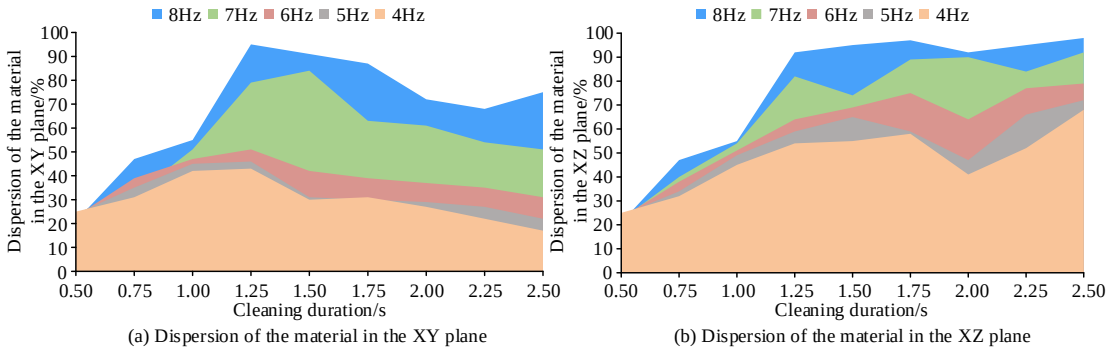


**Figure 6.** Comparison of the influence of different vibration frequencies on dispersion.

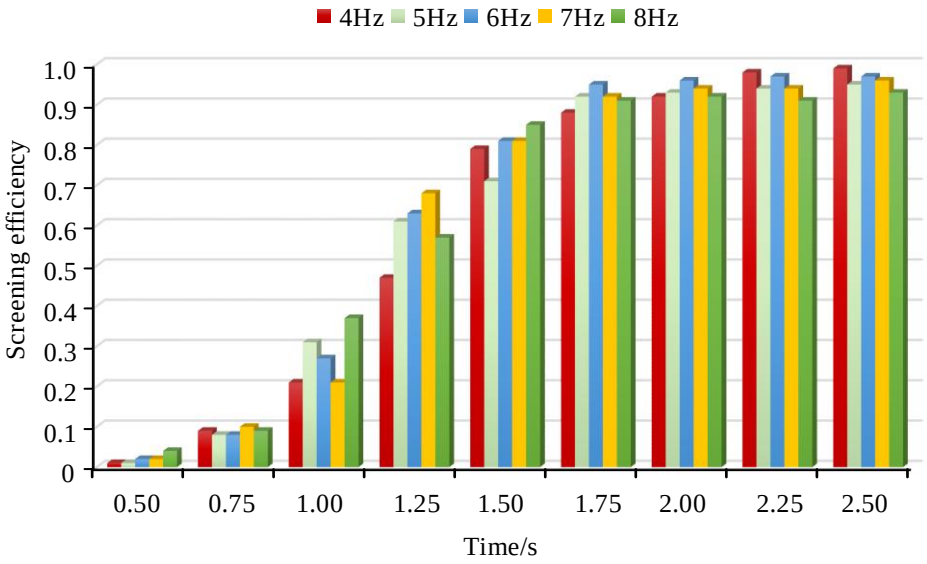


**Figure 7.** Comparison of the influence of different vibration frequencies on screening efficiency.

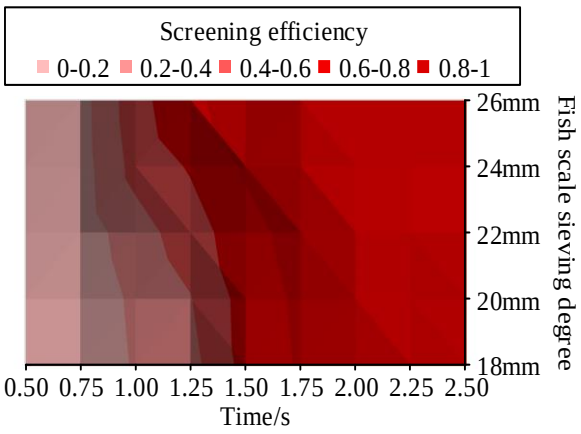


**Figure 8.** Comparison of the effect of fish scale sieving degree on sieving efficiency.

**The blocking quantity and impurity content of the modified fish scale sieve**

The improved fish scale sieve structure effectively solved the blockage problem with the blockage amount reduced by 63.7% compared to traditional fish scale sieves (Table 1). The impurity content had also been greatly improved, reaching a final impurity content of 1.4%, which was 81.3% improvement compared to that of traditional fish scale screens (Table 2).

In conventional mechanized corn harvesting, the separation efficiency of corn cleaning is low due to design defects in the equipment, and its separation degree is insufficient, resulting in high impurity content. Therefore, based on commonly

**Table 1.** Comparison of blockage of different fish scales.

| Fish scale sieve type | Experiment No. | Fish scale anterior ethmoid segment (g) | | Fish scale sieve middle (g) | | Fish scale end of sieve (g) | |
|---|---|---|---|---|---|---|---|
| Traditional fish scale sieve | 1 | 12.7 | 21.5 | 54.9 | 77.2 | 69.7 | 112.8 |
| | 2 | 11.8 | 22.1 | 56.1 | 76.7 | 66.7 | 111.9 |
| | 3 | 12.4 | 23.7 | 57.9 | 78.1 | 67.2 | 113.1 |
| | Average | 12.3 | 22.4 | 56.3 | 77.3 | 67.9 | 112.6 |
| | Total | 1046.5 | | | | | |
| Improved fish scale screen | 1 | 6.1 | 11.4 | 17.2 | 41.6 | 25.6 | 28.4 |
| | 2 | 2.4 | 12.7 | 15.3 | 42.8 | 22.7 | 29.7 |
| | 3 | 2.7 | 11.1 | 17.5 | 40.5 | 23.9 | 29.2 |
| | Average | 3.7 | 11.7 | 16.7 | 41.6 | 24.1 | 29.1 |
| | Total | 380.3 | | | | | |

**Table 2.** Comparison of impurity rate of different fish scales.

| Fish scale sieve type | Area | Grain weight through sieving (g) | Weight of sifted debris (g) | Impurity content (%) |
|---|---|---|---|---|
| Traditional fish scale sieve | Forepart | 6852.9 | 567.5 | 7.5 |
| | Midpiece | 14568.7 | 1010.8 | |
| | End piece | 4127.8 | 330.2 | |
| Improved fish scale screen | Forepart | 8927.6 | 165.4 | 1.4 |
| | Midpiece | 16792.9 | 297.6 | |
| | End piece | 5862.5 | 134.8 | |

used corn cleaning devices, an optimization of corn screening devices based on high-precision aerodynamic models was proposed from an aerodynamic perspective. The results of this study demonstrated that, when the wind speed was set at 16 m/s, the separation efficiency of corn was the highest, reaching 94.27%, and the screening efficiency also reached the highest, reaching 97.24%. When the vibration frequency of the device was set to 8 Hz, the separation performance of corn was the best, reaching a maximum of 97.24%. The optimal screening efficiency of 98.27% was achieved when the frequency was set to 4 Hz. When the opening of the fish scale sieve was set to 26 mm, the screening efficiency reached the best performance at 100%. The improved fish scale sieve performed well, and its material blockage had been greatly reduced by 63.7% compared to that of traditional fish scale sieves. The impurity content had also been greatly optimized with a final impurity content of 1.4%, which was 81.3% higher than that of a conventional fish-scale sieve. The results of this study confirmed that wind speed, vibration frequency, and the opening of the fish scale sieve all influenced the cleaning efficiency. The proposed corn screening device optimization based on high-precision aerodynamic model effectively solved material blockage in the cleaning device, greatly reduced the impurity content, and could provide positive assistance for the growth of corn production. However, the study did not consider the impact of different types of corn on the device, which should be investigated in further studies.

## Acknowledgements

The research was supported by the Natural Science Foundation of Xinjiang Uygur Autonomous Region (Grant No. 2022D01B138) and College Students Innovation and Entrepreneurship Training Program of Xinjiang

Uygur Autonomous Region (Grant No. S202210994013).

## References


1. Han J. 2020. Study on dynamic target positioning and grabbing based on binocular vision. Acad J Comput Inf Sci. 3(1):78-82.
2. Ji Y, Kumar R, Singh D, Singh M. 2021. Performance analysis of target information recognition system for agricultural robots. Int J Agric Environ Inf Syst. 12(2):49-60.
3. Wei SM, Li Y, Deng K, Lai HC, Tonetti MS, Shi JY. 2022. Does machine-vision-assisted dynamic navigation improve the accuracy of digitally planned prosthetically guided immediate implant placement? A randomized controlled trial. Clin Oral Implants Res. 33(8):804-815.
4. Ortiz-Peregrina S, Ortiz C, Casares-López M, Jiménez JR, Anera RG. 2021. Effects of cannabis on visual function and self-perceived visual quality. Sci Rep. 11(1):1-11.
5. Hu H, Kaizu Y, Zhang H, Xu Y, Imou K, Li M, *et al*. 2022. Recognition and localization of strawberries from 3D binocular cameras for a strawberry picking robot using coupled YOLO/Mask R-CNN. Int J Agric Biol Eng. 15(6):175-179.
6. Dong N, Meng F, Raffik R, Shabaz M, Neware R, Krishnan S, *et al*. 2022. Optimization of target acquisition and sorting for object-finding multi-manipulator based on open MV vision. Nonlinear Eng. 11(1):471-477.
7. Hsieh KW, Huang BY, Hsiao KZ, Tuan YH, Shih FP, Hsieh LC, *et al*. 2021. Fruit maturity and location identification of beef tomato using R-CNN and binocular imaging technology. J Food Meas Charact. 15(6):5170-5180.
8. Sverdlichenko I, Mandelcorn MS, Issashar Leibovitzh G, Mandelcorn ED, Markowitz SN, Tarita-Nistor L. 2022. Binocular visual function and fixational control in patients with macular disease: A review. Ophthalmic Physiol Opt. 42(2):258-271.
9. Wang F, Liu Q, Huang M, Qiao X, Huang Y. 2021. Research on sugarcane seed-bud location based on anisotropic scaling transformation. Appl Eng Agric. 37(6):1119-1130.
10. Wan G, Li F, Zhu W, Wang G. 2020. High-precision six-degree-of-freedom pose measurement and grasping system for large-size object based on binocular vision. Sens Rev. 40(1):71-80.
11. Li L. 2020. Research on target feature extraction and location positioning with machine learning algorithm. J Intell Syst. 30(1):429-437.
12. Zhu L, Zhang Y, Wang Y, Cheng C. 2022. Binocular vision positioning method for safety monitoring of solitary elderly. Comput Mater Contin. 71(1):593-609.
13. Jian X, Chen X, He W, Gong X. 2020. Outdoor 3D reconstruction method based on multi-line laser and binocular vision. IFAC-PapersOnLine. 53(2):9554-9559.
14. Wang L. 2021. Symbol recognition system based on 3D stereo vision. J Intell Fuzzy Syst. 40(4):5985-5994.
15. Gao H, Shen F, Zhang F, Zhang Z. 2022. A high precision and fast alignment method based on binocular vision. Int J Precis Eng Manuf. 23(9):969-984.
16. Xie Q, Hu X, Ren L, Qi L, Sun Z. 2022. A binocular vision application in IoT: realtime trustworthy road condition detection system in passable area. IEEE Trans Ind Inform. 19(1):973-983.
17. Sun Y, Liang L, Sun J, Chen X, Tian R, Chen Y, *et al*. 2022. A binocular vision SSVEP brain–computer interface paradigm for dual-frequency modulation. IEEE Trans Biomed Eng. 70(4):1172-1181.
18. Wang D, Sun H, Lu W, Zhao W, Liu Y, Chai P, *et al*. 2022. A novel binocular vision system for accurate 3-D reconstruction in large-scale scene based on improved calibration and stereo matching methods. Multimed Tools Appl. 81(18):26265-26281.
19. Niu J, Hu Q, Niu Y, Zhang T, Jha SK. 2021. Real-time recognition and location of indoor objects. Comput Mater Contin. 68(2):2221-2229.
20. Yin Z, Ren X, Du Y, Yuan F, He X, Yang F. 2022. Binocular camera calibration based on timing correction. Appl Opt. 61(6):1475-1481.
21. Wang X, Chen T, Wang Y, Zheng D, Chen X, Zhao Z. 2023. The 3D narrow butt weld seam detection system based on the binocular consistency correction. J Intell Manuf. 34(5):2321-2332.
22. Fang Q, Li H, Luo X, Li C, An W. 2020. A semantic and prior-knowledge-aided monocular localization method for construction-related entities. Comput-Aided Civ Infrastruct Eng. 35(9):979-996.